Review

Characterization of Catalytically Active Octahedral Metal Halide Cluster Complexes

Satoshi Kamiguchi [1,2,]*, Sayoko Nagashima [3] and Teiji Chihara [3]

[1] Organometallic Chemistry Laboratory, RIKEN, 2-1 Hirosawa, Wako City,
    Saitama 351-0198, Japan

[2] Advanced Catalysis Research Group, RIKEN Center for Sustainable Resource Science,
    2-1 Hirosawa, Wako City, Saitama 351-0198, Japan

[3] Graduate School of Science and Engineering, Saitama University, Shimo-Okubo, Sakura-Ku,
    Saitama City, Saitama 338-8570, Japan; E-Mails: nagasima@apc.saitama-u.ac.jp (S.N.);
    chihara@apc.saitama-u.ac.jp (T.C.)

* Author to whom correspondence should be addressed; E-Mail: kamigu@riken.jp;
    Tel.: +81-48-467-1349; Fax: +81-48-467-9391.

Abstract: Halide clusters have not been used as catalysts. Hexanuclear molecular halide clusters of niobium, tantalum, molybdenum, and tungsten possessing an octahedral metal framework are chosen as catalyst precursors. The prepared clusters have no metal–metal multiple bonds or coordinatively unsaturated sites and therefore required activation. In a hydrogen or helium stream, the clusters are treated at increasingly higher temperatures. Above 150–250 °C, catalytically active sites develop, and the cluster framework is retained up to 350–450 °C. One of the active sites is a Brønsted acid resulting from a hydroxo ligand that is produced by the elimination of hydrogen halide from the halogen and aqua ligands. The other active site is a coordinatively unsaturated metal, which can be isoelectronic with the platinum group metals by taking two or more electrons from the halogen ligands. In the case of the rhenium chloride cluster Re_3Cl_9, the cluster framework is stable at least up to 300 °C under inert atmosphere; however, it is reduced to metallic rhenium at 250–300 °C under hydrogen. The activated clusters are characterized by X-ray diffraction analyses, Raman spectrometry, extended X-ray absorption fine structure analysis, thermogravimetry–differential thermal analysis, infrared spectrometry, acid titration with Hammett indicators, and elemental analyses.

1. Introduction

One of the greatest challenges in catalysis is the development of new reactions over new catalysts. Our research on the application of halide cluster complexes to catalysis is reviewed.

Carbonyl clusters have been strongly associated with catalysis, as most of these clusters contain platinum group metals. These metals have versatile catalytic activities in both homogeneous and heterogeneous systems. However, carbonyl clusters are thermally unstable, and almost all decompose above 200 °C due to their inherently weak metal–metal bonds. This dissociation enthalpy for a metal–metal bond in a cluster is two-thirds of that of a metal–CO bond (terminal) [1]. Exceptionally, at >260 °C, $[PBu_4]_2[Os_{20}(CO)_{40}]$, which has a tetrahedral cubic close-packed (ccp) metal core of twenty Os atoms, was synthesized by the vacuum pyrolysis of $[Os_3(CO)_{10}(NCMe)_2]$ [2]. Hence, carbonyl cluster catalysis with retention of the cluster framework is difficult, and reactions catalyzed by coordinatively unsaturated carbonyl clusters with intact metal frameworks that have been isolated are rare [3]. Carbonyl clusters have been widely used as catalyst precursors for supported heterogeneous catalysts [4–6] or as models of metal catalysts [7,8]. In the latter cases, the carbonyl clusters afford uncoordinated metal species during the course of the reaction with or without decomposition of the metal frameworks, and the isolation and characterization of the adducts of carbonyl clusters with reactants are fairly easy.

Another type of cluster complex is known. The first report of the synthesis of a halide cluster, $MoCl_2$, was published in 1859 [9] (Figure 1). Early on, it was considered to be a trimer; however, the definitive hexameric structure was established by X-ray analysis in 1967 as Mo_6Cl_{12} or, more exactly, $[Mo_6Cl^i_8]Cl^a_2Cl^{a-a}_{4/2}$ [10], where "*i*" and "*a*" refer to the inner and outer (auβer) coordination spheres, respectively, and "*a-a*" refers to the corresponding linkage between two clusters. Extensive efforts have been directed at the synthesis of new halide clusters or the combination of known halide clusters with new networks. Presently, more than a hundred types of halide clusters have been synthesized by combining nineteen kinds of Group 3–7 metal atoms and four kinds of π-donor halogen ligands [11–13]. Halide clusters are generally synthesized by the comproportionation of a metal with a corresponding mononuclear metal halide at elevated temperatures (typically 600–1300 °C) for several days to weeks in a sealed tube as solid-state clusters. Then, the molecular clusters are synthesized by scission heat-treating with ligands or π-donor solvents (Figure 1). As the metal–metal bonds of the Groups 5 and 6 (4d and 5d) metals are stronger than their platinum group counterparts, an uncoordinated metal center can be revealed if some of the ligands are removed, leaving the thermally stable metal framework intact. Most halide clusters have octahedral metal array structures, consisting of the pure metal crystals with terminally coordinating, bridging, or triply bridging halogen π-donor ligands (Figure 2). These halide clusters have several characteristic features. The clusters are characterized by the middle oxidation states (1+ to 3+) of the metal atoms, which are intermediate between those of the bulk metal and the metal oxide. The catalytic activity, as well as the reactivity, of the metal atoms in the middle oxidation states,

have not been reported. Moreover, the concerted effects of the metal–metal bonds of the cluster are also unknown. In multi-center and multi-electron systems, polynuclear coordination could induce reactivity in a ligand that differs significantly from that produced by mononuclear coordination [14]. Thermal stability is the largest advantage of the halide clusters over carbonyl clusters, and halide clusters have low vapor pressures and high melting points as halide complexes. Halide clusters have solid (network) and molecular states, which can be used in heterogeneous and homogeneous systems. A diversity of metal atoms and halogen ligands is also an attribute of halide clusters.

Figure 1. Structure of solid-state molybdenum chloride cluster Mo_6Cl_{12} ($[Mo_6Cl^i_8]Cl^a_2Cl^{a-a}_{4/2}$) and molecular clusters $(H_3O)_2[(Mo_6Cl_8)Cl_6]\cdot 6H_2O$, $[(Mo_6Cl_8)Cl_4(H_2O)_2]\cdot 6H_2O$, and $[(Mo_6Cl_8)Cl_4(H_2O)_2]$.
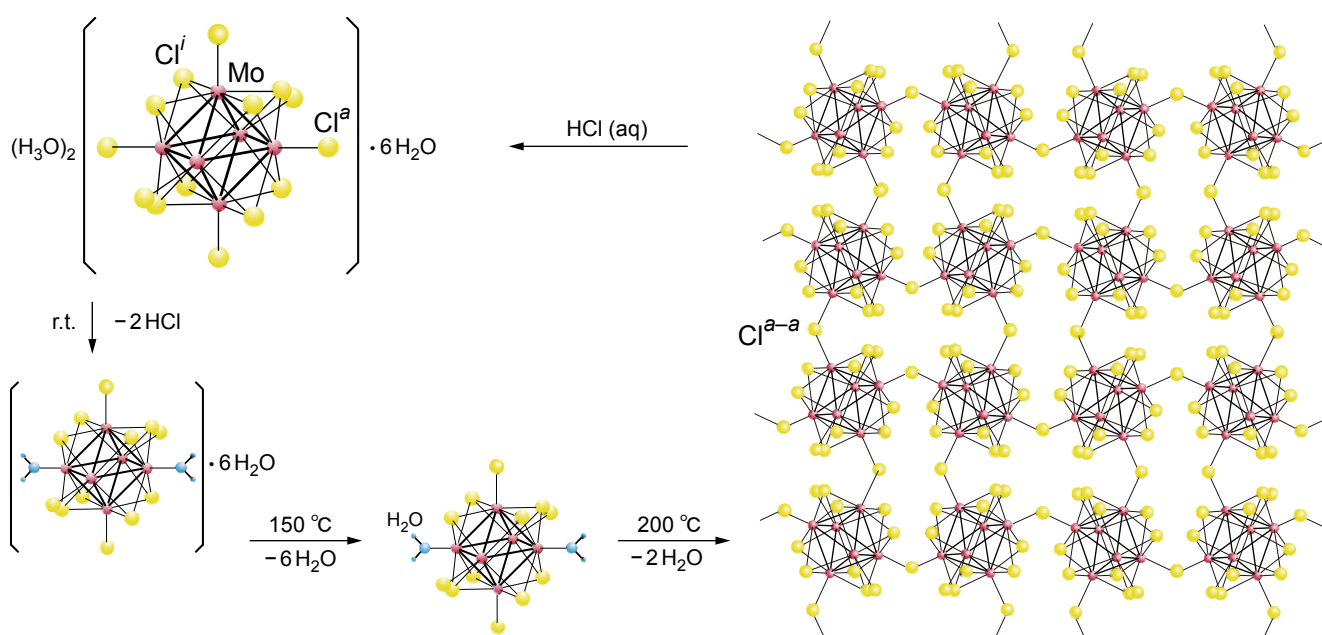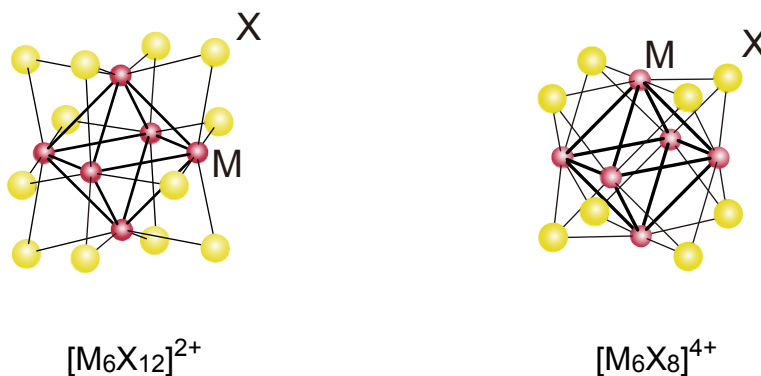

Figure 2. Two basic structures of halide clusters. Halogen π-donor ligands coordinate in two modes as inner ligands: 12 halogen ligands in a μ_2-fashion in $[M_6X_{12}]^{2+}$, and eight halogen ligands in a μ_3-fashion in $[M_6X_8]^{4+}$.


$[M_6X_{12}]^{2+}$

$[M_6X_8]^{4+}$

Studies on the reactivity of halide clusters are quite limited, and have generally been confined to observations of ligand exchange reactions with organic or inorganic reagents, an exception being the report of a simple reaction with hydrogen [15,16]. The applications of these clusters have been explored

based on properties such as high temperature superconductivity, metallic conductivity at elevated temperatures, low-dimensional electronic or magnetic properties, and good thermal stability. Halide clusters are promising candidates for catalysts [17]; however, only $MoCl_2$ has been used as a catalyst precursor, although the integrity of the cluster was destroyed during use [18].

The synthesized clusters have no metal–metal multiple bonds or coordinatively unsaturated sites, and accordingly, they are not active catalyst as they stand. Pretreatment for activation is necessary. In the case of a liquid batch-reaction system, the elimination of a halogen ligand by basic reagents or silver(I) ions results in the development of catalytic activity. However, this method is not applicable in a gas–solid reaction system, in which there are no restrictions on the reaction temperature. Therefore, activation in the gas phase has been attempted. The ligands of the coordination complexes are in equilibrium with free molecules or ions, although the dissociation constant is quite low at room temperature. In the case of the molecular molybdenum chloride cluster $[(Mo_6Cl_8)Cl_4(H_2O)_2]$, the ligands can be removed as neutral molecules at elevated temperatures in the gas phase. Plausible reactions for the activation are given by equations in Figure 3. As shown in Figure 3, a halide cluster was placed in a gas stream to avoid the recoordination of a liberated ligand, and heated gradually to dissociate or change the ligands until catalytic activity developed. Retention of the cluster framework was expected.

Figure 3. Activation and plausible reactions of a halide cluster in a gas stream with increasing temperature.
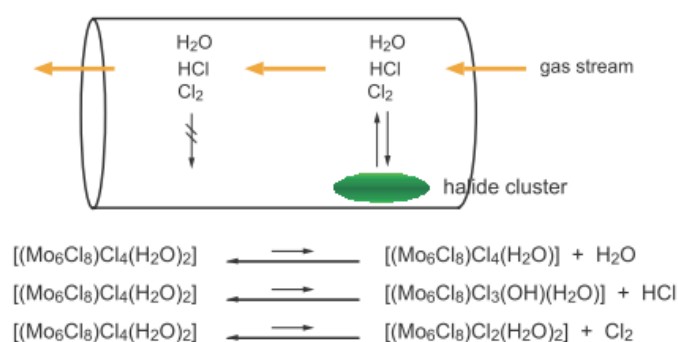
To date, nineteen Groups 3–7 transition metal atoms have been reported to afford halide cluster complexes. The electronegativities of the Groups 3 and 4 transition metals are low and it is difficult to remove the coordinated oxygen atoms of ligands from the cluster complexes. This suggests that oxygen-containing reactants cannot be applied for catalysis. In the case of Groups 6 and 7 transition metals, the coordinated oxygen atoms of ligands can be removed by heating above 200 °C. The preparation of Groups 3 and 4 metal clusters are not easy, since the syntheses are performed in a niobium or tantalum sealed tube. In contrast, Groups 5–7 metal clusters can be synthesized easily, and the clusters are stable in air. Oxygen- or nitrogen-containing reactants can be used over Groups 5–7 metals because of their moderate affinities. Thus, Groups 5–7 transition metal cluster complexes with chlorine ligands were chosen for study as potential catalysts.
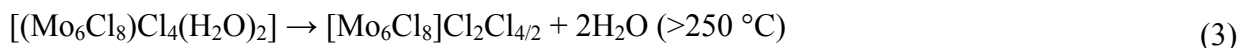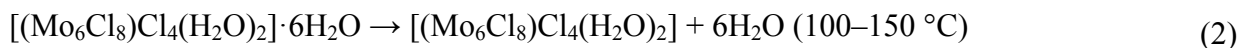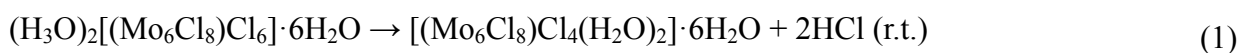
Halide clusters, the majority of which have a highly symmetrical and aesthetically pleasing $[M_6X_8]$ or $[M_6X_{12}]$ unit [19], are attractive catalyst candidates. Since the synthesis of halide clusters was first reported over 150 years ago [9], they have been dormant to catalysis, like a "Sleeping Beauty". In recent

years, we have reported a series of reactions catalyzed by these clusters. This review is concerned with the activation and characterization of these cluster catalysts.

2. Activation and Characterization of Cluster Complexes Containing Group 6 Metals

2.1. Retention of the Cluster Framework of the $(H_3O)_2[(Mo_6Cl_8)Cl_6]\cdot 6H_2O$ Molybdenum Cluster [20]

The undiluted crystalline powder of the molybdenum halide cluster $(H_3O)_2[(Mo_6Cl_8)Cl_6]\cdot 6H_2O$ in a glass reaction tube was heated in a helium stream for 1 h at elevated temperature. The X-ray diffraction (XRD) patterns of samples treated at various temperatures are illustrated in Figure 4, in addition to that of independently synthesized $[Mo_6Cl^i_8]Cl^a_2Cl^{a-a}_{4/2}$. The cluster chemistry of $MoCl_2$ has been extensively investigated. The XRD pattern of $(H_3O)_2[(Mo_6Cl_8)Cl_6]\cdot 6H_2O$ treated at ambient temperature for 1 h exactly matches that of $[(Mo_6Cl_8)Cl_4(H_2O)_2]\cdot 6H_2O$. In this reaction, two Cl ligands in the starting complex are removed as HCl, yielding the aqua complex $[(Mo_6Cl_8)Cl_4(H_2O)_2]\cdot 6H_2O$ (Equation (1)). This complex loses its water of crystallization by treatment at 100–150 °C affording $(H_3O)_2[(Mo_6Cl_8)Cl_6]$ (Equation (2)). The evolution of Cl_2 was not detected at this stage. The XRD patterns of samples treated above 250 °C reveal conversion into an extended Mo–Cl–Mo bonded solid-state cluster $[Mo_6Cl_8]Cl_2Cl_{4/2}$ (Equation (3)). The half-band widths of the peaks at 12.6° and 15.6° grow narrower when the sample is heated from 250 to 400 °C, indicating an increasing crystallinity with increasing treatment temperature.

$$(H_3O)_2[(Mo_6Cl_8)Cl_6]\cdot 6H_2O \rightarrow [(Mo_6Cl_8)Cl_4(H_2O)_2]\cdot 6H_2O + 2HCl \text{ (r.t.)} \tag{1}$$

$$[(Mo_6Cl_8)Cl_4(H_2O)_2]\cdot 6H_2O \rightarrow [(Mo_6Cl_8)Cl_4(H_2O)_2] + 6H_2O \text{ (100–150 °C)} \tag{2}$$

$$[(Mo_6Cl_8)Cl_4(H_2O)_2] \rightarrow [Mo_6Cl_8]Cl_2Cl_{4/2} + 2H_2O \text{ (>250 °C)} \tag{3}$$

The Raman spectra of the heat-treated samples are shown in Figure 5, in which some of the assigned peaks for the molecular cluster $(H_3O)_2[(Mo_6Cl_8)Cl_6]\cdot 6H_2O$ are indicated. The Raman spectra of halide clusters are generally insensitive to ligand exchange. For example, the Raman spectrum of $(C_6H_5CH_2NMe_3)_2[(Mo_6Cl_8)Cl_6]$ is quite similar to that of $[(Mo_6Cl_8)Cl_4(THF)_2]$ [21]. This observation demonstrates that the change in the outer ligands from a Cl to an oxygen donor does not grossly affect the symmetry of the molecule. The spectra of $(H_3O)_2[(Mo_6Cl_8)Cl_6]\cdot 6H_2O$ and the samples treated up to 150 °C are very similar; and four assigned peaks are retained. Above 200 °C, the Raman peak originally at 321 cm^{-1} ascribed to the triple-bridged Mo–Cl^i breathing vibration was replaced by two peaks, suggesting a change in the coordination mode, and a new peak appeared at 278 cm^{-1}. Catalytic activity for various reactions emerged at 200 °C. The spectra of the samples treated at 200–600 °C are quite similar to that of authentic $[Mo_6Cl^i_8]Cl^a_2Cl^{a-a}_{4/2}$ prepared by the reported method [22]. Thus, the results from Raman spectrometry accord with the discussion of the XRD analyses after treatment from room temperature to 600 °C.

Figure 4. XRD patterns of $(H_3O)_2[(Mo_6Cl_8)Cl_6]\cdot6H_2O$ treated at various temperatures in a helium stream for 1 h. The XRD pattern of authentic Mo_6Cl_{12} is also shown. All the identified compounds have two strong diffraction peaks at 12.4°–12.6° and 15.3°–15.6°. Unique diffraction peaks for each compound are indicated: (**a**) for $(H_3O)_2[(Mo_6Cl_8)Cl_6]\cdot6H_2O$; (**b**) for $[(Mo_6Cl_8)Cl_4(H_2O)_2]\cdot6H_2O$; (**c**) for $[(Mo_6Cl_8)Cl_4(H_2O)_2]$; and (**d**) for Mo_6Cl_{12}.
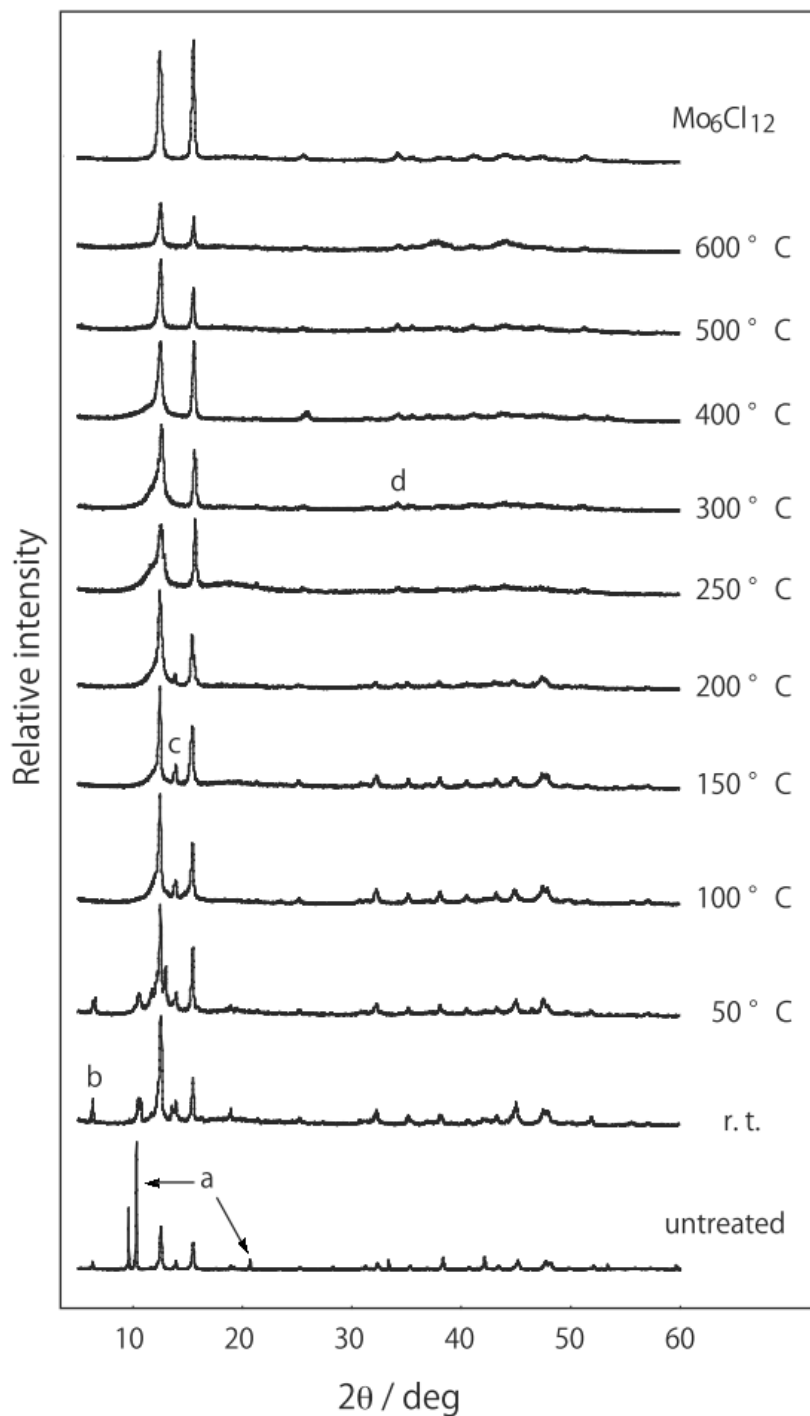
Figure 5. Raman spectra of $(H_3O)_2[(Mo_6Cl_8)Cl_6]\cdot 6H_2O$ treated at various temperatures in a helium stream for 1 h. The Raman spectrum of authentic Mo_6Cl_{12} is also shown.
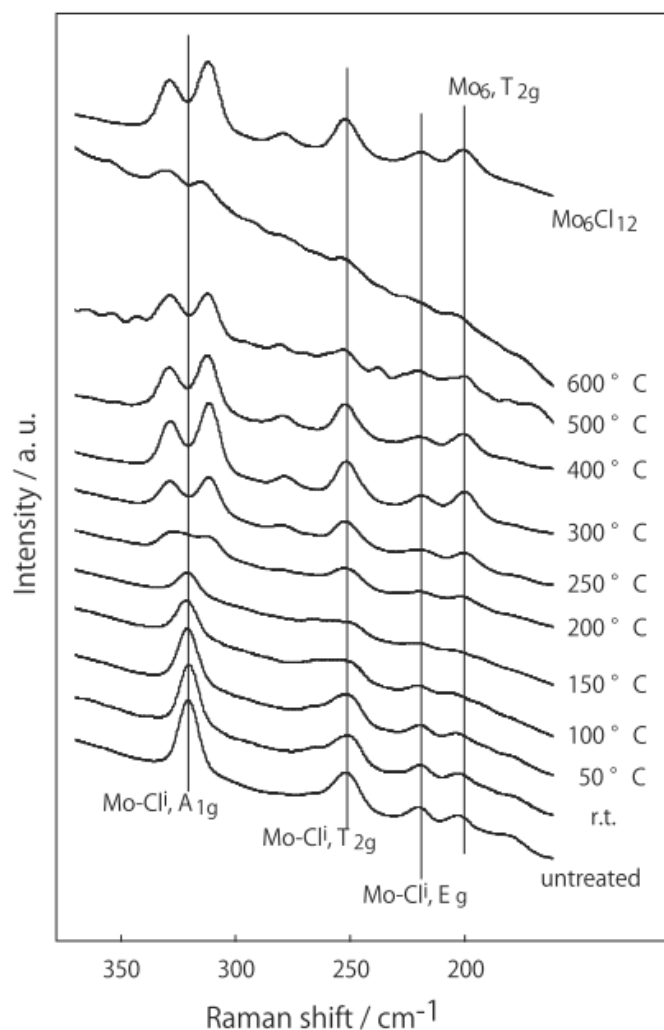
The extended X-ray absorption fine structure (EXAFS) spectra of the near Mo K-edge absorption region for the treated samples are shown in Figure 6a, and the values of the coordination number (C.N.) for Mo–Mo and the bond length determined by curve fitting are plotted in Figure 6b. Only small changes were observed in the EXAFS spectra for treatment up to 400 °C. The value of C.N. for Mo–Mo, which corresponds to the Mo_6 octahedron, was unchanged up to 400 °C. The Mo–Mo distance of the cluster framework was also retained up to 450 °C. These findings accord with the change in $(H_3O)_2[(Mo_6Cl_8)Cl_6]\cdot 6H_2O$ via $[(Mo_6Cl_8)Cl_4(H_2O)_2]\cdot 6H_2O$ and $[(Mo_6Cl^i_8)Cl^a_4(H_2O)_2]$ to $[Mo_6Cl^i_8]Cl^a_2Cl^{a\text{-}a}_{4/2}$, all of which have the same C.N. and Mo–Mo distance, and, hence, prove that the 400 °C-treated sample retained the Mo_6 cluster framework. Treatment above 450 °C caused a significant decrease in both the C.N. and Mo–Mo distance. The decreasing intensity of the XRD peaks above 500 °C, as shown in Figure 4, is attributable to the partial decay of $[Mo_6Cl^i_8]Cl^a_2Cl^{a\text{-}a}_{4/2}$. No appreciable changes in the EXAFS spectra were observed after subsequent 3 h reaction with diethylamine at 400 °C; the bond distance and the C.N. for Mo–Mo were 0.261 ± 0.002 nm and 4.2 ± 0.4, respectively, after the reaction. This C.N. of the Mo–Mo bond, corresponding to the octahedral metal framework, indicates the retention of the cluster framework throughout the reaction. Thus, these results clearly show the retention

of the Mo cluster framework and face-capping Cl ligands during the treatment and the catalytic reaction at 400 °C or above under helium. Under hydrogen, retention of the cluster framework of Mo with face-capping Cl ligands in $(H_3O)_2[(Mo_6Cl_8)Cl_6]\cdot6H_2O$ has similarly been confirmed up to 400 °C [23].

Figure 6. (**a**) The k^3-weighted EXAFS oscillations at the Mo K-edge for $(H_3O)_2[(Mo_6Cl_8)Cl_6]\cdot6H_2O$ treated at various temperatures in a helium stream for 1 h, and (**b**) values of coordination number (C.N.,○) and bond length (*R*, ●) determined by curve fitting.
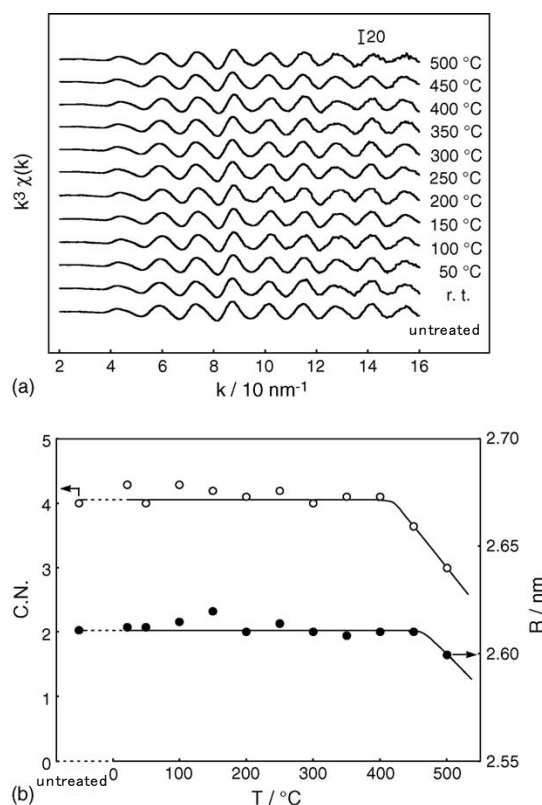
2.2. Active Site of Molybdenum Cluster

Figure 7 shows the thermogravimetry–differential thermal analysis (TG–DTA) profiles of $(H_3O)_2[(Mo_6Cl_8)Cl_6]\cdot6H_2O$ under hydrogen [24]. The DTA data showed an endothermic peak from ambient temperature to 60 °C. The total weight loss of 5% corresponds to the loss of hydrogen chloride from the anionic cluster $(H_3O)_2[(Mo_6Cl_8)Cl_6]\cdot6H_2O$ to yield the neutral cluster $[(Mo_6Cl_8)Cl_4(H_2O)_2]\cdot6H_2O$ (Equation (1)). The subsequent endothermic weight loss of 8% from 60 to 117 °C is attributable to the loss of the water of crystallization from $[(Mo_6Cl_8)Cl_4(H_2O)_2]\cdot6H_2O$ (Equation (2)). The next endothermic weight loss above 117 °C can be attributed to the loss of aqua ligands to yield the solid state molybdenum cluster $[Mo_6Cl_8]Cl_2Cl_{4/2}$ (Equation (3)). However, the evolution of hydrogen chloride was detected above 117 °C and a gradual weight loss was observed from ~190 °C to approximately 450 °C. Hence, by rapid heating, $(H_3O)_2[(Mo_6Cl_8)Cl_6]\cdot6H_2O$ could be decomposed by other routes, as exemplified by Equations (4) and (5).

$$[(Mo_6Cl_8)Cl_4(H_2O)_2] \rightarrow [(Mo_6Cl_8)Cl_3(OH)(H_2O)] + HCl \; (>190\ °C) \tag{4}$$

$$[(Mo_6Cl_8)Cl_3(OH)(H_2O)] \rightarrow [(Mo_6Cl_8)Cl_2(OH)_2] + HCl \ (>190 \ °C) \tag{5}$$
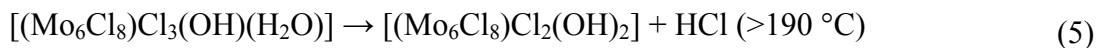
Figure 7. TG and DTA profiles of $(H_3O)_2[(Mo_6Cl_8)Cl_6]\cdot6H_2O$.
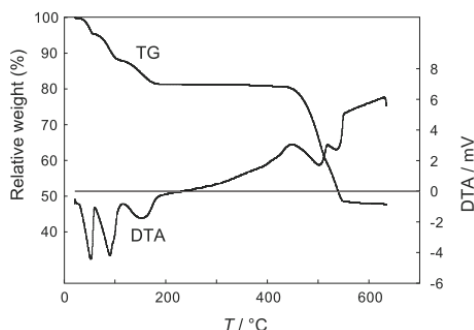
Closer examination of the XRD patterns illustrated in Figure 4 shows that the crystallinity of the heat-treated $(H_3O)_2[(Mo_6Cl_8)Cl_6]\cdot6H_2O$ was poor. This indicated that the coordinated water had not been completely removed by the pretreatment, and that the oxygen of the water molecules had been captured. Elemental analysis of the sample treated at 400 °C in a helium stream revealed that it consisted of Mo (57.6 wt%) and Cl (40.5 wt%), with a residue (1.9 wt%) originating from the coordinated water. These findings can be interpreted in terms of the formation of an imperfect crystal including the defective $\{[Mo_6Cl_8]Cl^a_2Cl^{a-a}_{4/2}\}$ moiety. That is to say, the catalytically active cluster moiety that has a hydroxo ligand such as $\{[Mo_6Cl^i_8]Cl^a_2Cl^{a-a}_{3/2}(OH)\}$ or $\{[Mo_6Cl^i_8]Cl^aCl^{a-a}_{4/2}(OH)\}$ was retained intact in the imperfect crystal lattice of the solid-state cluster, as illustrated in Figure 8. The hydroxo ligands would dissociate H^+ as expressed by Equation (6).
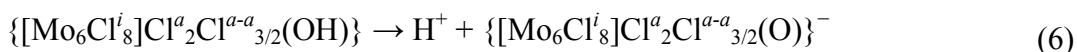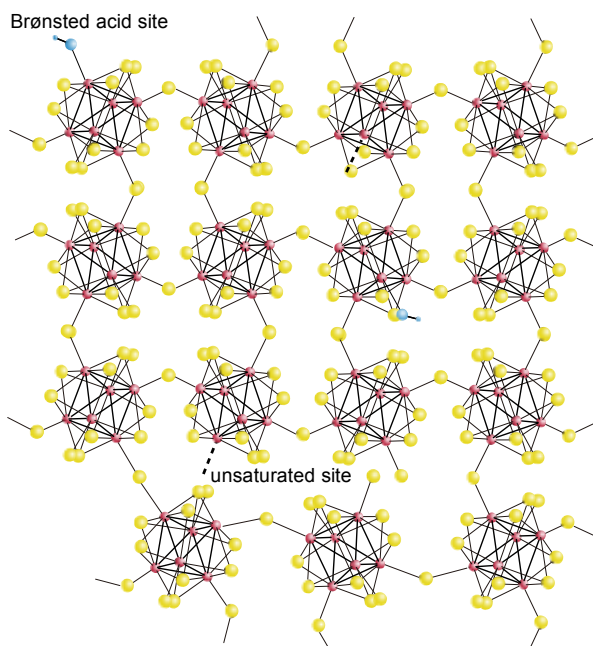
$$\{[Mo_6Cl^i_8]Cl^a_2Cl^{a-a}_{3/2}(OH)\} \rightarrow H^+ + \{[Mo_6Cl^i_8]Cl^a_2Cl^{a-a}_{3/2}(O)\}^- \tag{6}$$

Figure 8. Active sites formed in the imperfect crystal lattice of the solid state cluster Mo_6Cl_{12}.

A hydroxo cluster of molybdenum, $[(Mo_6Cl_8)Cl_2(OH)_2(H_2O)_2]$, has been reported to be a weak acid, affording protons in aqueous solution [25]. Consequently, the development of Brønsted acid sites in the poorly crystallized solid-state cluster retaining hydroxo ligands was expected.

A complete description of surface acidity requires the determination of acid strength and the number of acid centers. The titration method cannot be applied to the crushed crystals of $(H_3O)_2[(Mo_6Cl_8)Cl_6]\cdot 6H_2O$, as it changes to a deeply colored crystal upon heat treatment [24]. Therefore, the acidity of $(H_3O)_2[(Mo_6Cl_8)Cl_6]\cdot 6H_2O$ supported on silica gel (380 m^2/g) in 5.0 wt%, $(H_3O)_2[(Mo_6Cl_8)Cl_6]\cdot 6H_2O/SiO_2$, was measured using the *n*-butylamine titration method with various Hammett indicators [26]. Figure 9 plots *n*-butylamine titers as a function of the Hammett acidity function (H_0). The titer for each plot corresponds to the number of acid sites with acid strengths equal to or greater than the H_0 value. No acidity was observed for $(H_3O)_2[(Mo_6Cl_8)Cl_6]\cdot 6H_2O/SiO_2$ treated at 150 °C under hydrogen. Treatment at 300 °C resulted in acidity development. In contrast to the crystalline cluster, almost all of the supported cluster molecules on SiO_2 were exposed and could not be converted to the solid-state cluster $[Mo_6Cl^i_8]Cl^a_2Cl^{a-a}_{4/2}$. The supported clusters activated at 300 °C exhibited an equimolar number of acid sites at $H_0 \approx 1.3$ with an additional equimolar number of acid sites at $H_0 \approx 1.5$–2.0. These two acid sites can be attributed to the first and second dissociations of protons from the hydroxo ligands of $[(Mo_6Cl_8)Cl_2(OH)_2]$, as exemplified by Equation (6). These sharp distributions of the acid strength and the equivalence of the acid sites on the cluster molecules are characteristic of a molecular catalyst, as solid acids such as silica-alumina and zeolites have a wide distribution of acid strengths because of their inhomogeneous structures. The H_0 values of H_3BO_3 and H_3PO_4 supported on silica gel at 0.1 mmol g^{-1} are reported to be +1.3 to +1.5 and +1.5 to −3.0, respectively [27].

Figure 9. *n*-Butylamine titers *versus* acid strength for $(H_3O)_2[(Mo_6Cl_8)Cl_6]\cdot 6H_2O/SiO_2$ treated at 150 °C (Δ) and 300 °C (○) in a hydrogen stream. The titer for the same amount of the SiO_2 support treated at 300 °C (■) is also shown.
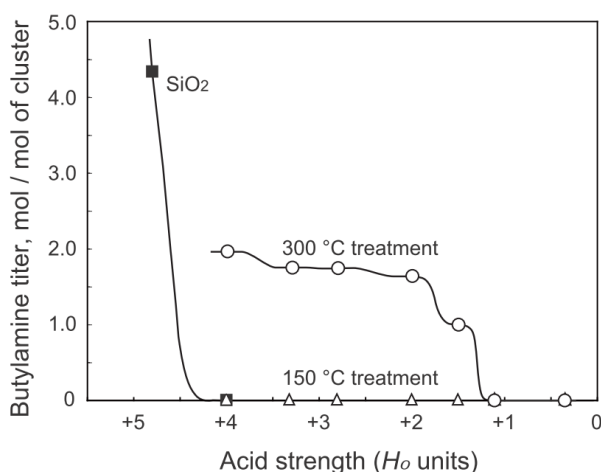
The solid-phase synthesis of the well-formed crystalline solid state cluster $[Mo_6Cl_8]Cl^a_2Cl^{a-a}_{4/2}$ is achieved by slowly raising the temperature (over 2 h) of the crystalline molecular cluster $(H_3O)_2[(Mo_6Cl_8)Cl_6]\cdot 6H_2O$ to 200 °C, followed by heating (for 5+ h) at 200 °C under vacuum to constant weight, as illustrated in Figure 1 [22]. In this process, the coordinated water of the intermediate

$[(Mo_6Cl_8)Cl_4(H_2O)_2]$ is removed and replaced with a bridging $Cl^{a\text{-}a}$ ligand. Rapid heating to higher temperatures, as employed for activation, leads to the formation of a poorly crystallized solid-state cluster containing defective $[Mo_6Cl_8]Cl^a_2Cl^{a\text{-}a}_{4/2}$ moieties, in which molybdenum atoms without bridging $Cl^{a\text{-}a}$ ligands can be formed. In other words, a coordinatively unsaturated molybdenum atom would be formed by such activation, and would function as the active site of the cluster catalyst. Titration with CO revealed that 0.167 eq. of CO was adsorbed on $(H_3O)_2[(Mo_6Cl_8)Cl_6]\cdot6H_2O/SiO_2$, when the sample had been treated at 300 °C.

The incorporation of dihydrogen into cluster complexes has been reported in the literature. Halide clusters can take up dihydrogen to yield $ThI_2H_{0.7}$, $Nb_6I_{11}H_{1.3}$, or $Mo_6Cl_{12}H_{0.7}$ at temperatures between 150 and 450 °C [15]. Dihydrogen directly converts double-metal-layered ZrX (X = Cl and Br) to the ZrXH phase [16].

Figure 10. Isoelectronic relationships between catalyst metals. In the area of solid metal catalysis, researchers inspect the periodic table longitudinally to find other catalytically active metals for the relevant reaction, as the number of d-electrons plays an important role in catalysis. Iron, ruthenium, and osmium are catalytically active metals for the synthesis of ammonia. In the areas of molecular and complex catalyses, researchers also examine the periodic table laterally, as ligands change the valence electron distribution of the metal atom and sometimes change its electron distribution, such that the metal becomes isoelectronic with that of the rightward metal atoms in the periodic table.
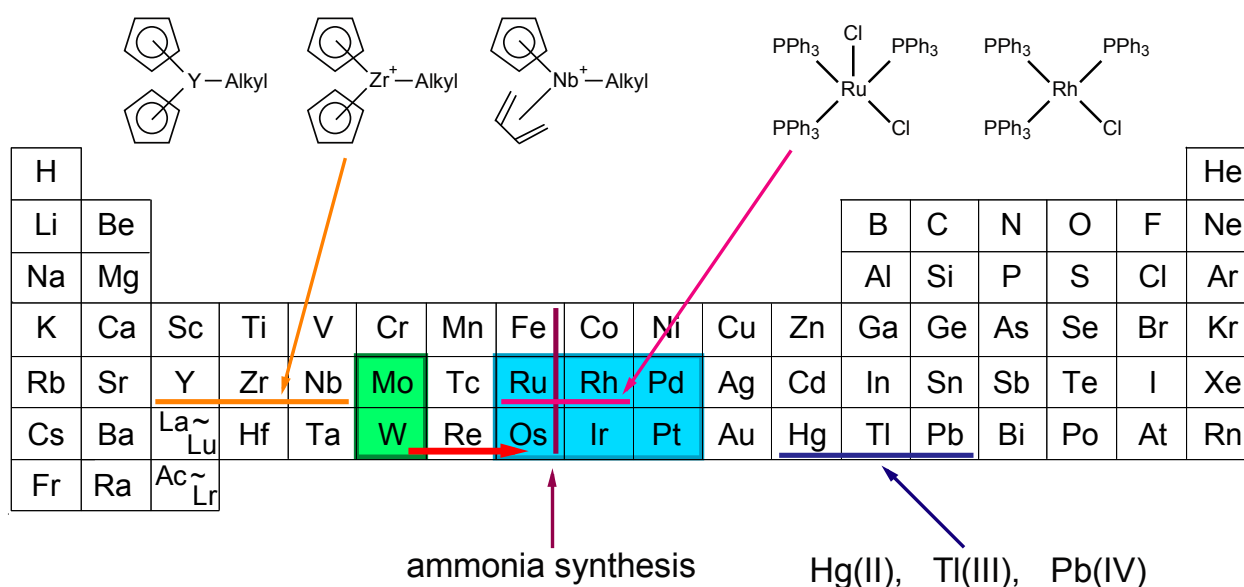

Therefore, we deduced that a coordinatively unsaturated or, under hydrogen, a hydrido-coordinated Mo atom would be formed as a component of the Mo_6 cluster framework, and would be the active site of the cluster catalyst. Isoelectronic metal atoms occasionally exhibit the same catalysis as is exemplified by the nitration of alkylbenzenes catalyzed by Hg(II), Tl(III), or Pb(IV) (Figure 10) [28]. A series of $Y(\eta^5\text{-}C_5H_5)_2(alkyl)$, $[Zr(\eta^5\text{-}C_5H_5)_2(alkyl)]^+$, and $[Nb(\eta^5\text{-}C_5H_5)(\eta^4\text{-}C_4H_6)]^+$ moieties show similar polymerization activity [29]. It is well known that Ru metals in $[RuCl_2(PPh_3)_3]$ and $[RuHCl(PPh_3)_3]$ are isoelectronic with Rh metal in $[RhCl(PPh_3)_3]$, and that these complexes catalyze the hydrogenation of olefinic bonds [30]. The carbides and nitrides of niobium, molybdenum, and tungsten exhibit similar

catalysis to iridium metal for hydrazine decomposition in the thruster engines of satellites [31]. This has been explained by the addition of the ligand atom's valence electrons to the metal atoms, which affords an electron distribution similar to that of the iridium metal. Consequently, the coordinatively unsaturated or hydrido-coordinated Mo metal atom in the activated molybdenum cluster could be isoelectronic with the platinum group metals by taking two or more electrons from the halogen ligands, and might catalyze hydrogenation, dehydrogenation, and hydrodehydration.

### 2.3. Tungsten Cluster $(H_3O)_2[(W_6Cl_8)Cl_6] \cdot 6H_2O$

The activation behavior of the tungsten halide cluster $(H_3O)_2[(W_6Cl_8)Cl_6] \cdot 6H_2O$, also based on a Group 6 transition metal, is quite similar to that of the isomorphous molybdenum cluster $(H_3O)_2[(Mo_6Cl_8)Cl_6] \cdot 6H_2O$ under both hydrogen [32] and helium [33] streams. One of the differences is the order of the loss of ligands and the transformation temperatures: water of crystallization is lost by treatment at 50 °C to yield $(H_3O)_2[(W_6Cl_8)Cl_6]$, and then two apical chloro ligands are lost by treatment above 100 °C to afford $[(W_6Cl_8)Cl_4(H_2O)_2]$. When the cluster is heated progressively, it changes to an extended W–Cl–W-bonded solid-state compound $[W_6Cl^i_8]Cl^a_2Cl^{a-a}_{4/2}$ at 250–300 °C. The other difference is that the activated defective solid-state cluster $[W_6Cl^i_8]Cl^a_2Cl^{a-a}_{4/2}$ is stable to temperatures as high as 400 °C under hydrogen [32] and 450 °C under helium [33].

The development of a Brønsted acid site on $(H_3O)_2[(W_6Cl_8)Cl_6] \cdot 6H_2O/SiO_2$ was ascertained by measuring the IR spectra of adsorbed pyridine [34]. The IR spectrum of $(H_3O)_2[(W_6Cl_8)Cl_6] \cdot 6H_2O/SiO_2$ treated at 450 °C in a hydrogen stream followed by the adsorption of pyridine is illustrated in Figure 11. A band at 1445 cm^{-1} attributable to pyridine hydrogen-bonded to surface silanol groups is common in each spectrum. The two bands at 1540 and 1489 cm^{-1}, assignable to pyridinium ion in the spectrum of $(H_3O)_2[(W_6Cl_8)Cl_6] \cdot 6H_2O/SiO_2$ both before and after the reaction, show the presence of a Brønsted acid site on $(H_3O)_2[(W_6Cl_8)Cl_6] \cdot 6H_2O$. However, there is no band that is characteristic of coordinatively bonded pyridine in the 1449–1460 cm^{-1} region, and hence, there is no Lewis acid site. Hydroxo or oxo species developed in imperfect crystals of $[W_6Cl_8]Cl_2Cl_{4/2}$ by treatment at 450 °C exhibited Brønsted acidity, as expressed in Equation (7).

$$[(W_6Cl_8)Cl_2(OH)_2] \rightarrow H^+ + [(W_6Cl_8)Cl_2(OH)(O)]^- \tag{7}$$
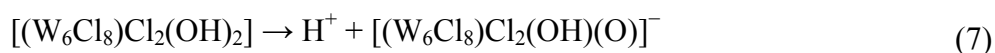
In summary, when the molybdenum and tungsten clusters were treated with progressively increasing temperatures, they lost two apical chlorido ligands and water of crystallization to yield $[(Mo_6Cl_8)Cl_4(H_2O)_2]$ and $[(W_6Cl_8)Cl_4(H_2O)_2]$ up to 200 °C. Then they were transformed to poorly crystallized solid-state clusters containing active sites which comprised Brønsted acid sites and coordinatively unsaturated sites that are stable to 400–450 °C with retention of the cluster framework.

Figure 11. IR spectra of pyridine adsorbed on $(H_3O)_2[(W_6Cl_8)Cl_6]\cdot 6H_2O/SiO_2$. Sample powder (15 mg) was pressed into a disk (10 mm diameter) and treated in a hydrogen stream at 450 °C for 1 h (**A**), followed by introduction of pyridine (**B**). Catalyst sample after 4 h of reaction of toluene with methanol (**C**) and unsupported silica gel (**D**) were treated in the same way.
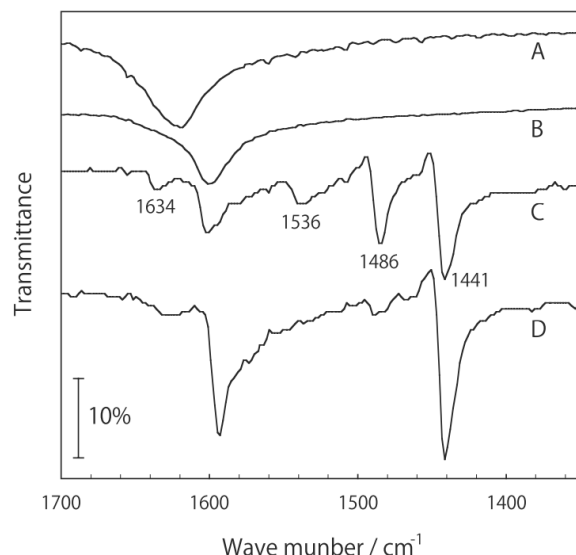
3. Activation and Characterization of Cluster Complexes Containing Group 5 Metals

3.1. Retention of the Cluster Framework of the Niobium Cluster [(Nb₆Cl₁₂)Cl₂(H₂O)₄]·4H₂O [20]

The undiluted crystal powder of the niobium halide cluster $[(Nb_6Cl_{12})Cl_2(H_2O)_4]\cdot 4H_2O$ in a glass reaction tube was treated in a helium stream for 1 h at an elevated temperature. The XRD patterns of the treated samples at various temperatures are depicted in Figure 12. The changes in the pattern reveal that treatment above 100 °C transformed the cluster into an amorphous compound due to the loss of water of crystallization (Equation (8)).

$$[(Nb_6Cl_{12})Cl_2(H_2O)_4]\cdot 4H_2O \rightarrow [(Nb_6Cl_{12})Cl_2(H_2O)_4] + 4H_2O \ (>100\ ^\circ C) \tag{8}$$
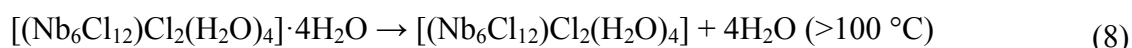
The evolution of HCl gas was detected when the cluster was treated above 150 °C, and a violent evolution began when treated above 200 °C. However, Cl_2 gas was not detected up to 500 °C. The amorphous compound was not the extended solid-state cluster Nb_6Cl_{14} ($[Nb_6Cl^i_{10}Cl^{i\text{-}a}_{2/2}]\ Cl^{a\text{-}i}_{2/2}Cl^{a\text{-}a}_{4/2}$) that was prepared by the direct reaction of Nb metal with $NbCl_5$ [35].

The Raman spectra of the heat-treated samples under helium are shown in Figure 13. The spectra markedly changed at 250 °C with increasing temperature. The band at 239 cm^{-1} is assigned to the breathing motion of the Nb_6 octahedron (A_{1g}), and those at 161 and 152 cm^{-1} are attributed to edge bridging Nb–Cl^i breathing vibrations (E_g and T_{2g}, respectively) [36]. Crystal structural data revealed that the differences in M–M distances parallel the observed variations in the Raman shift [37]. The variations in the observed shift of the M_6 A_{1g} band are almost entirely accounted for by differences in the M–M force constant that accompany changes in the M–M bond distances [37]. The band of the Nb_6 A_{1g} vibration mode begins to shift to higher energy upon treatment and has a maximum shift at 250 °C. The loss of some ligands can increase the Nb–Nb bond order of the Nb_6 octahedron, which may be ascribed

to the higher energy shift [37]. Nevertheless, the Nb_6 metal framework remains intact. Above 250 °C the two Raman bands originally at 161 and 152 cm^{-1} due to edge-bridging Nb–Cl^i breathing vibrations are replaced with a new band, which suggests that the coordination mode of the ligands changes above this temperature. Loss of the Cl atom as HCl was detected and the origin of the H atom in HCl can be an aqua ligand. No appreciable changes in the Raman spectra were observed after 3 h catalytic reaction with phenyl acetate at 150 °C. The Raman spectra of the samples heat-treated under hydrogen were the same as those treated under helium [32].

Figure 12. XRD patterns of $[(Nb_6Cl_{12})Cl_2(H_2O)_4]\cdot 4H_2O$ treated at various temperatures in a helium stream for 1 h.
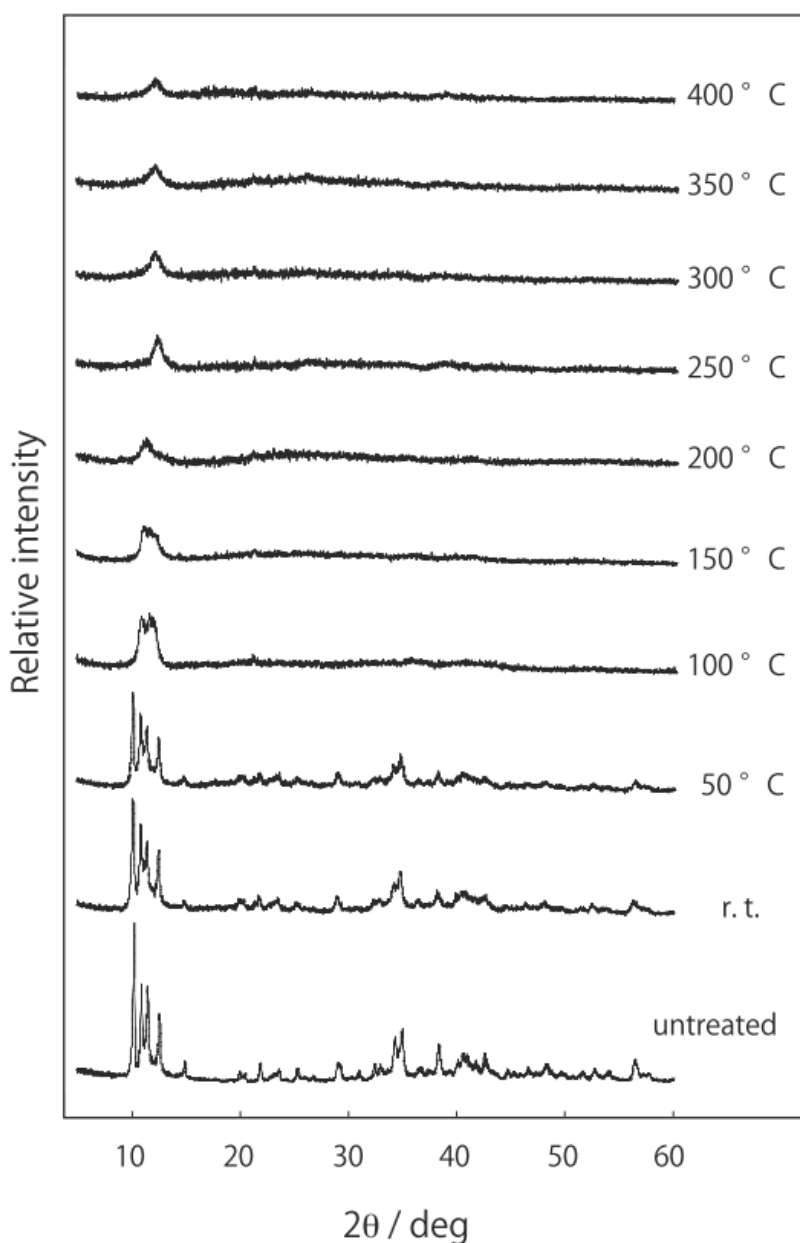
Figure 13. Raman spectra of $[(Nb_6Cl_{12})Cl_2(H_2O)_4] \cdot 4H_2O$ treated at various temperatures in a helium stream for 1 h.
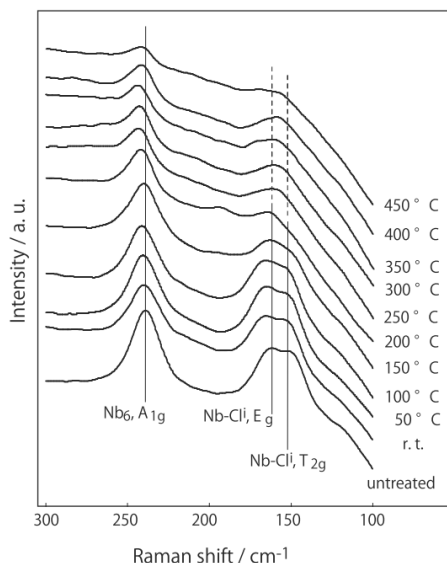
The EXAFS spectra of the near Nb K-edge absorption region for the helium-treated samples, and the Nb−Nb C.N. values and bond lengths determined by curve fitting are plotted in Figure 14. The Nb−Nb bond length of 0.291 nm, which corresponds to the Nb_6 octahedron, was maintained up to 400 °C and the C.N. values for Nb−Nb were retained up to 250 °C with increasing treatment temperature. Accordingly, the octahedral cluster framework was completely retained to 250 °C, then began to disintegrate with increasing temperature, and disintegrated above 400 °C.

Figure 14. The k^3-weighted EXAFS oscillations at the Nb K-edge for $[(Nb_6Cl_{12})Cl_2(H_2O)_4] \cdot 4H_2O$ treated at various temperatures in a helium stream for 1 h, and (**b**) values of coordination number (C.N., ○) and bond length (*R*, ●) determined by curve fitting.
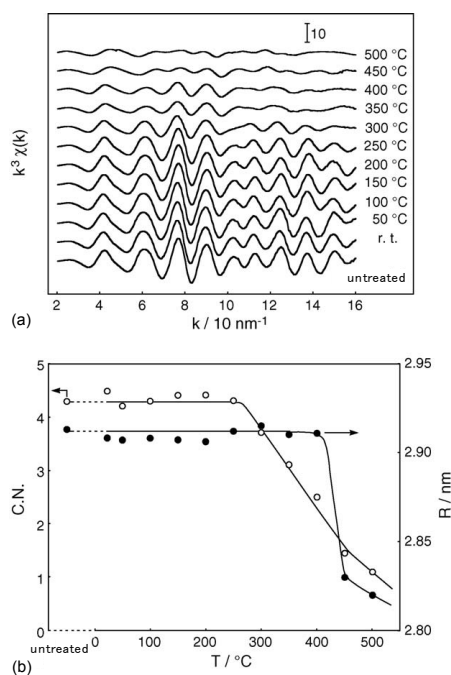
The elemental analysis data for the Nb and Cl atoms in the treated samples revealed that the Cl content of $[(Nb_6Cl_{12})Cl_2(H_2O)_4]\cdot 4H_2O$, and consequently the relative amount of Cl to Nb, definitely decreased above 200 °C with increasing treatment temperature. The origin of the hydrogen in the liberated hydrogen chloride was the aqua ligand. Assuming that the remainder was composed of hydroxyl groups, the $Nb_6Cl_{11.2}(OH)_{4.8}$ species, on average, was formed by treatment at 250 °C. Since the outer halogen ligands are generally labile, and, hence, are replaced prior to the inner ligands, the loss of the inner Cl ligands commenced at this stage, which is consistent with the results obtained by Raman and IR (Section 3.1) analyses. Above this temperature, the substantial loss of the Cl ligand began. Thus, when $[(Nb_6Cl_{12})Cl_2(H_2O)_4]\cdot 4H_2O$ was treated with progressively increasing temperature, its crystal structure decayed above 100 °C by the loss of water of crystallization (Equation (8)). Loss of the Cl ligand began above 150 °C with retention of the Nb_6 cluster framework. Above 400 °C, the Nb_6 octahedron practically decayed.

3.2. Active Site of Niobium Cluster

The TG curve for $[(Nb_6Cl_{12})Cl_2(H_2O)_4]\cdot 4H_2O$ illustrated in Figure 15 shows a clear two-step weight loss [33]. The ~7% weight loss and associated endothermic effect between ambient temperature and 150 °C can be ascribed to the loss of the crystallization water (Equation (8)). A large weight loss between 150 and 250 °C was observed in the TG analysis. The DTA curve indicates a large exothermic effect. Evolution of HCl was observed when $[(Nb_6Cl_{12})Cl_2(H_2O)_4]\cdot 4H_2O$ was treated above 150 °C. The bond energy of O–H (427.6 kJ mol^{-1}) is comparable to that of Cl–H (431.6 kJ mol^{-1}). The bond energy of Nb–O (771.5 kJ mol^{-1}) is fairly large, though no data has been reported for that of Nb–Cl. The electronegativity of niobium is greater than that of chlorine. The exothermic effect is attributable to the oxidation of the niobium atom. Accordingly, the 22.5% weight loss between 150 and 250 °C corresponds to the loss of hydrochloric acid from the aqua and chloro ligands to form the hydroxo clusters (Equations (9) and (10)).

$$[(Nb_6Cl_{12})Cl_2(H_2O)_4] \rightarrow [(Nb_6Cl_{12})Cl(OH)(H_2O)_3] + HCl \ (150\text{–}250 \ °C) \tag{9}$$

$$[(Nb_6Cl_{12})Cl(OH)(H_2O)_3] \rightarrow [(Nb_6Cl_{12})(OH)_2(H_2O)_2] + HCl \ (150\text{–}250 \ °C) \tag{10}$$
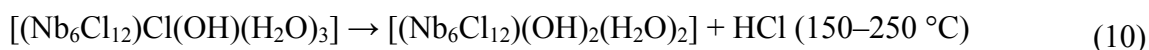
Figure 15. TG and DTA profiles of $[(Nb_6Cl_{12})Cl_2(H_2O)_4]\cdot 4H_2O$.
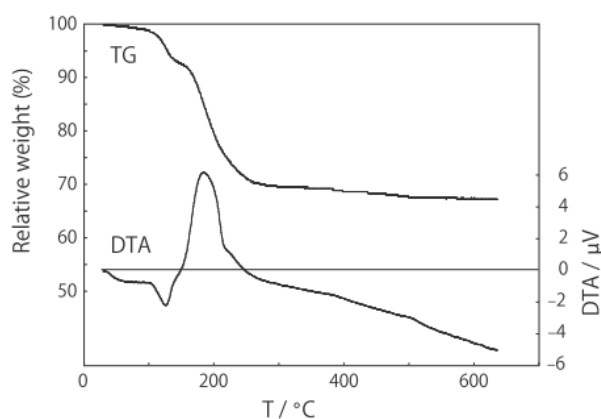
The diffuse reflectance FT-IR spectra of $[(Nb_6Cl_{12})Cl_2(H_2O)_4] \cdot 4H_2O$ treated at various temperatures are presented in Figure 16 [38]. All the samples exhibited O–H stretching vibrations in the region of 3600 cm^{-1}, suggesting the retention of the hydroxy group even after the reaction of aniline with acetone at 300 °C for 3 h. In the region of 397 cm^{-1}, the Nb_6–OH stretching vibration of a hydroxo ligand appears upon treatment, whereas the Nb_6–OH$_2$ stretching vibration of an aqua ligand exhibits no peaks. As exemplified by Equations (9) and (10), a hydroxo ligand appears upon treatment above 250 °C and is retained after the reaction of aniline with acetone at 300 °C for 3 h, indicating the conservation of the hydroxo cluster.

Figure 16. IR spectra of $[(Nb_6Cl_{12})Cl_2(H_2O)_4] \cdot 4H_2O$ treated at various temperatures in a hydrogen stream for 1 h. IR spectrum of $[(Nb_6Cl_{12})Cl_2(H_2O)_4] \cdot 4H_2O$ subjected to 3 h reaction of aniline with acetone at 300 °C is also shown.
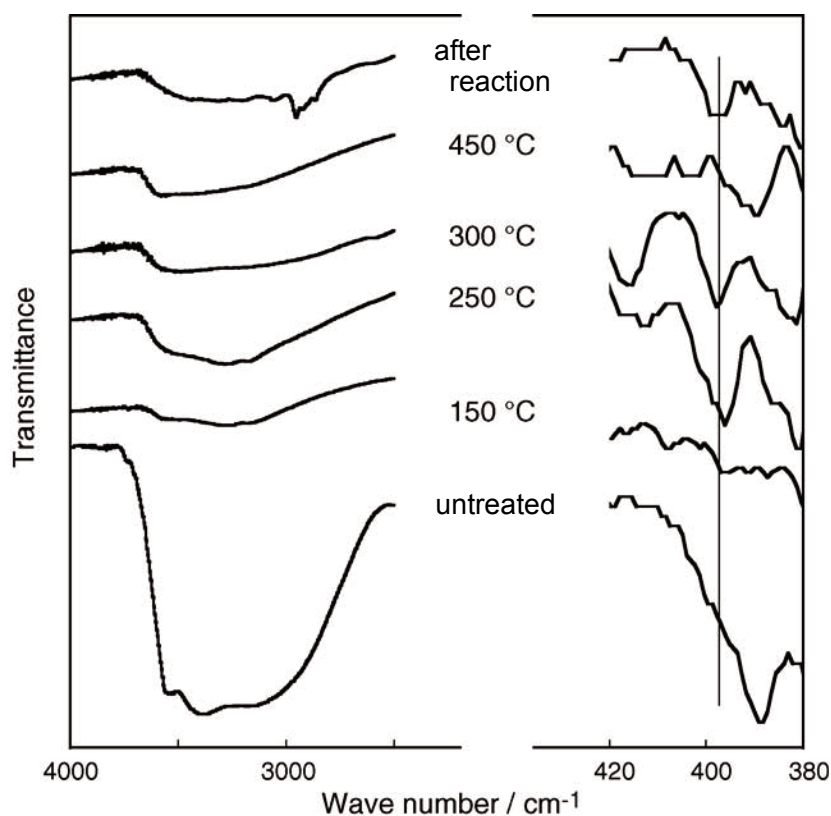
Then, the appearance of the acid site was detected. The IR spectrum of crystalline $[(Nb_6Cl_{12})Cl_2(H_2O)_4] \cdot 4H_2O$ treated at 250 °C in a helium stream followed by the adsorption of pyridine is illustrated in Figure 17 [20]. The band at 1441 cm^{-1} was assigned to a hydrogen bonded pyridine, as untreated $[(Nb_6Cl_{12})Cl_2(H_2O)_4] \cdot 4H_2O$ has water of crystallization and aqua ligands. Three bands at 1634, 1536, and 1486 cm^{-1} assignable to pyridinium ion in the spectrum of $[(Nb_6Cl_{12})Cl_2(H_2O)_4] \cdot 4H_2O$ treated at 250 °C show the presence of a Brønsted acid site. Furthermore, there is no band that is characteristic of coordinatively bonded pyridine in the 1447–1460 cm^{-1} region, and, hence, there is no Lewis acid site.

Figure 17. IR spectra of pyridine adsorbed on $[(Nb_6Cl_{12})Cl_2(H_2O)_4] \cdot 4H_2O$. Crystals of $[(Nb_6Cl_{12})Cl_2(H_2O)_4] \cdot 4H_2O$ (**A**) were treated in a helium stream at 250 °C for 1 h (**B**), followed by introduction of pyridine (**C**). Pyridine was introduced to the crystals of $[(Nb_6Cl_{12})Cl_2(H_2O)_4] \cdot 4H_2O$ without thermal activation (**D**).
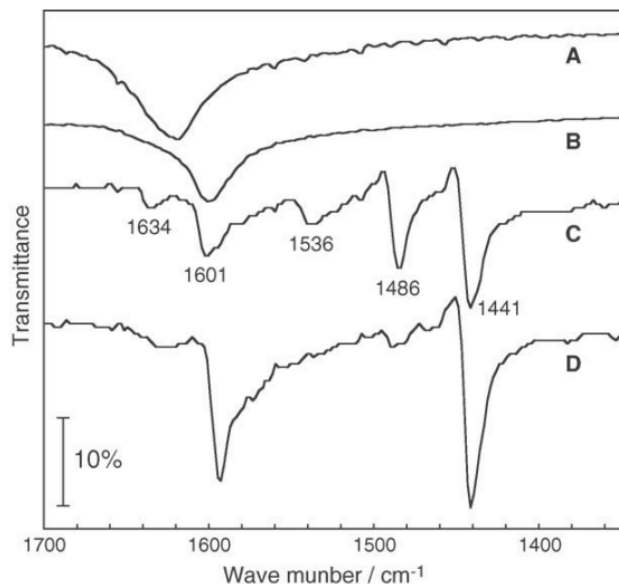
The acidity of $[(Nb_6Cl_{12})Cl_2(H_2O)_4] \cdot 4H_2O/SiO_2$ was measured using the *n*-butylamine titration method with various Hammett indicators. The cluster activated at 150 °C exhibited an equimolar number of acid sites at $1.1 < H_0 \le 1.5$. The acid sites can be attributed to the dissociation of protons from the hydroxo ligands of $[(Nb_6Cl_{12})(OH)_2(H_2O)_2]$, as exemplified by Equation (11). No acidity in $[(Nb_6Cl_{12})Cl_2(H_2O)_4] \cdot 4H_2O/SiO_2$ was observed without thermal treatment. No acid sites with an H_0 stronger than +4.0 were detected on the silica gel support.

$$[(Nb_6Cl_{12})(OH)_2(H_2O)_2] \rightarrow H^+ + [(Nb_6Cl_{12})(OH)(O)(H_2O)_2]^- \qquad (11)$$
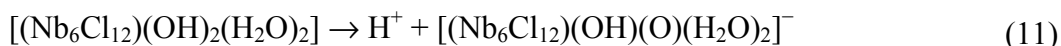
The activation behavior of the niobium cluster under a hydrogen stream is almost the same as that under helium streams [32]. Hydrogen served to physically rather than chemically remove the produced H_2O and HCl. The activation behavior of a tantalum halide cluster $[(Ta_6Cl_{12})Cl_2(H_2O)_4] \cdot 4H_2O$, also a Group 5 transition metal, is quite similar to that of the isomorphous niobium cluster $[(Nb_6Cl_{12})Cl_2(H_2O)_4] \cdot 4H_2O$ under both helium and hydrogen streams [39]. Formation of Brønsted acid sites was confirmed, and no basic sites were detected by CO_2 adsorption on the activated tantalum cluster. The tantalum cluster was rather thermally stable.

In summary, the active sites of niobium and tantalum clusters are Brønsted acid sites that are stable to 350–400 °C with retention of the cluster framework. The formation of coordinatively unsaturated sites seems more difficult than for molybdenum and tungsten clusters, since removal of the coordinated oxygen atoms of the aqua ligands is difficult even under a hydrogen stream because of the large bond dissociation enthalpies of Nb–O (771.5 kJ mol^{-1}) and Ta–O (799.1 kJ mol^{-1}).

3.3 Rhenium Cluster Re₃Cl₉ ([Re₃Clⁱ₃]Clᵃ₃Clᵃ⁻ᵃ₆/₂)

The XRD patterns of the powdered crystals of the rhenium halide cluster Re_3Cl_9 treated at various temperatures in helium streams for 1 h are shown in Figure 18, and the Raman spectra of these samples are illustrated in Figure 19 [40]. The crystal structure and unit cell dimensions of Re_3Cl_9 were retained up to 400 °C, while the crystallinity decreased above 350 °C. The Raman spectrum noticeably changed on treatment at 300 °C. At this temperature, the peaks attributable to the Re–Cl and Re–Re vibration modes nearly disappeared. The samples treated at 350 °C and 400 °C were notable because they mostly maintained the original crystal structure but the constituents were no longer the same as those of Re_3Cl_9. This apparent disagreement can be interpreted by the partial decomposition of the component cluster $[Re_3Cl_9]$ unit, which remains in the same position of the crystal lattice. The generation of Cl_2 gas was not detected throughout the treatment. However, the slight evolution of HCl gas was observed at the vent when Re_3Cl_9 was treated in a stream of helium at 150 °C, and strong evolution began when treated above 200 °C.

Figure 18. XRD patterns of Re_3Cl_9 treated at various temperatures under a helium stream for 1 h. Top pattern is that of Re_3Cl_9 treated in a hydrogen stream for 1 h at 300 °C showing reduction of Re_3Cl_9 to metallic rhenium.
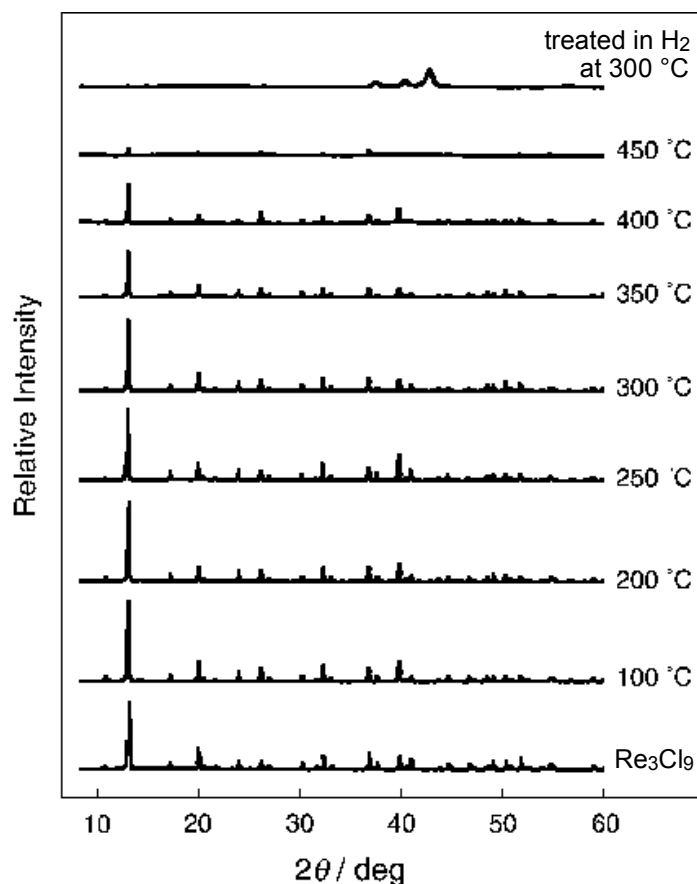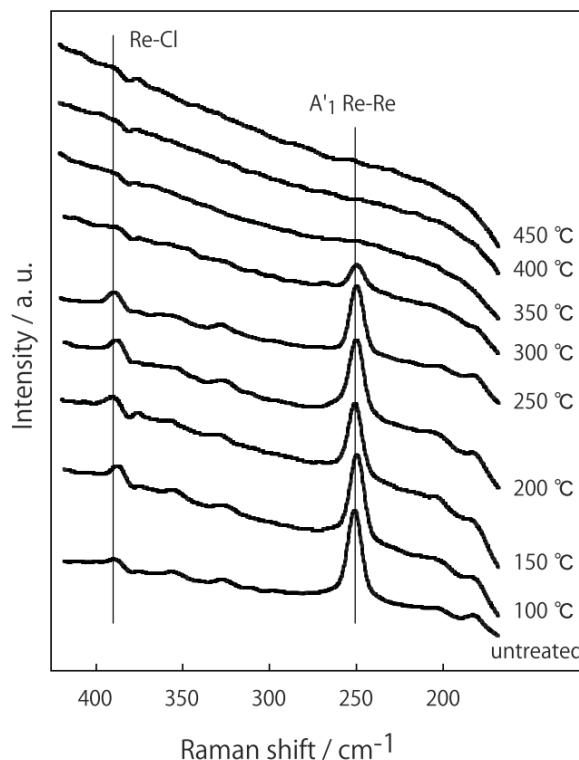
Figure 19. Raman spectra of Re_3Cl_9 treated at various temperatures under helium for 1 h.


It is difficult to dissolve the freshly prepared solid-state cluster Re_3Cl_9 ($[Re_3Cl^i_3]Cl^a_3Cl^{a-a}_{6/2}$), which consists of a $[Re_3Cl^i_3]Cl^a_3$ moiety linked by weak halide bridges $Cl^{a-a}_{6/2}$ (Figure 20). However, after exposure to a solvent followed by removal of the solvent, the materials becomes much more soluble in many solvents. This is due to the initial disruption of the tight Re_3Cl_9 structure, which remains disrupted after removal of the first solvent [41]. The Re_3Cl_9 cluster can be thermally stable for a short time at up to 450 °C, at which temperature it can be purified by vacuum sublimation, presumably by breaking the $Cl^{a-a}_{6/2}$ cluster bridges in the solid state. Although Re_3Cl_9 decomposes in aqueous solution, it reacts with a number of Lewis bases with retention of the triangular metal framework to form complexes of the type $L_3Re_3Cl_9$, where L = triphenylphosphine, pyridine, *etc*. [42]. Trace amounts of water contained in the reaction system could be incorporated in this solid cluster as coordinated water. Hence, Re_3Cl_9 can be activated by treatment under a stream of helium to form Re–OH or Re–O species, as expressed in Equations (12)–(14).

$$Re_3Cl_9 + H_2O \rightarrow Re_3Cl_9(H_2O) \tag{12}$$

$$Re_3Cl_9(H_2O) \rightarrow Re_3Cl_8(OH) + HCl \tag{13}$$

$$Re_3Cl_8(OH) \rightarrow Re_3Cl_7O + HCl \tag{14}$$

Thus, the catalytically active site of the rhenium cluster would be attributed to the acid site of the metal–OH moiety (hydroxo cluster) or metal–O moiety (oxo cluster) with retention of the metal cluster framework, which is stable at least up to 300 °C under inert atmosphere. Additionally, a coordinatively unsaturated site can be developed by removal of the chloro ligands or by breaking the $Cl^{a-a}_{6/2}$ cluster

bridges in the solid state. Under hydrogen, in contrast, the cluster is reported to be reduced to metallic rhenium at 250–300 °C, which has been confirmed by XRD analysis (Figure 18).

Figure 20. Structure of Re_3Cl_9 ($[Re_3Cl^i_3]Cl^a_3Cl^{a-a}_{6/2}$).
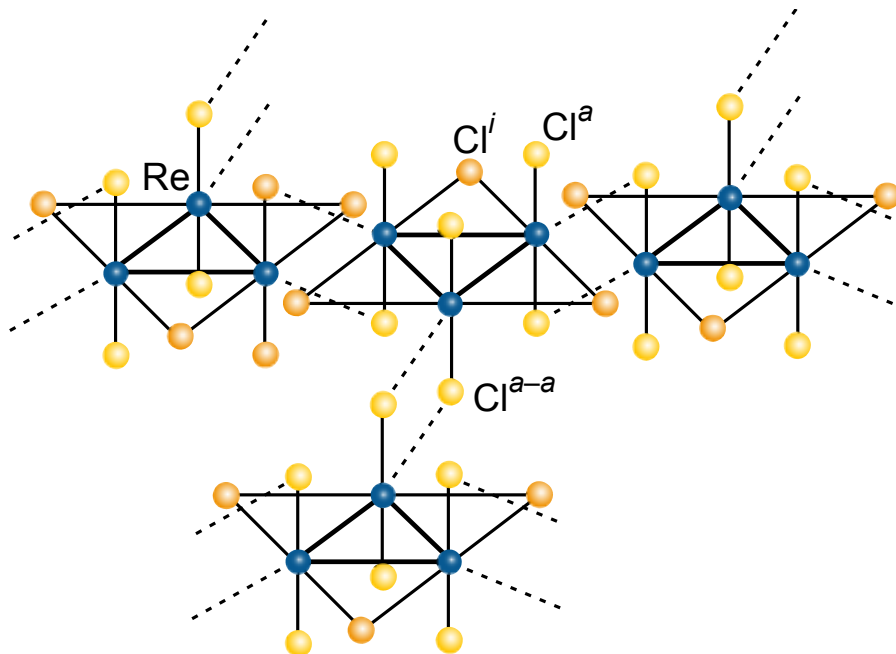
4. Conclusions

When molecular halide clusters of niobium, tantalum, molybdenum, and tungsten ($[(M_6X_{12})X_2(H_2O)_4]\cdot 4H_2O$ (M = Nb, Ta; X = Cl, Br), $(H_3O)_2[(M_6X_8)X_6]\cdot 6H_2O$ (M = Mo, W; X = Cl, Br)) possessing octahedral metal frameworks are treated in a hydrogen or helium stream, the metal framework is retained up to 350–450 °C. Above 150–250 °C, two kinds of catalytically active sites develop in the clusters. One is a weak Brønsted acid resulting from a hydroxo ligand that is formed by the elimination of hydrogen halide from the halogen and aqua ligands. The other is a coordinatively unsaturated metal atom formed by the removal of an aqua ligand. This coordinatively unsaturated metal atom in the cluster could be isoelectronic with the platinum group metals by taking two or more electrons from the halogen ligands. Thus, activated halide clusters of Groups 5 and 6 metals are a bi-functional catalysts. In the case of the rhenium chloride cluster Re_3Cl_9, the cluster framework is stable to at least 300 °C under inert atmosphere; however, it is reduced to metallic rhenium at 250–300 °C under hydrogen. Catalytic reactions that occur over halide clusters will be presented in the subsequent paper [43].

Conflicts of Interest

The authors declare no conflict of interest.

References

1. Mingos, D.M.P.; Wales, D.J. *Introduction to Cluster Chemistry*; Prentice-Hall: Upper Saddle River, NJ, USA, 1990; p. 6.

2. Gade, L.H.; Johnson, B.F.G.; Lewis, J.; McPartlin, M.; Powell, H.R.; Raithby, P.R.; Wong, W.T. Synthesis and structural characterisation of the osmium cluster dianions $[Os_{17}(CO)_{36}]^{2-}$ and $[Os_{20}(CO)_{40}]^{2-}$. *J. Chem. Soc. Dalton Trans.* **1994**, *1994*, 521–532.

3. Chihara, T.; Yamazaki, H. Hexaruthenium carbido carbonyl methyl cluster $[PPN][Ru_6C(CO)_{16}(CH_3)]$ as catalyst precursor for hydrogenation of olefins. Syntheses and structures of unsaturated and saturated hexaruthenium hydrido clusters $[PPN][Ru_6C(CO)_{15}H]$ and $[PPN][Ru_6C(CO)_{16}H]$. *J. Organomet. Chem.* **1994**, *473*, 273–284.

4. Lamb, H.H. Engineering catalyst surfaces with metal carbonyl clusters. *Catal. Today* **1993**, *18*, 3–19.

5. Braunstein, P.; Rosé, J. Heterometallic clusters for heterogeneous catalysis. In *Catalysis by Di- and Polynuclear Metal Cluster Complexes*; Adams, R.D., Cotton, F.A., Eds.; Wiley-VCH: New York, NY, USA, 1998; Chapter 13, p. 443.

6. Gates, B.C. Metal cluster catalysts dispersed on solid supports. In *Catalysis by Di- and Polynuclear Metal Cluster Complexes*; Adams, R.D., Cotton, F.A., Eds.; Wiley-VCH: New York, NY, USA, 1998; Chapter 14, p. 509.

7. Zuffa, J.L.; Gladfelter, W.L. On the mechanism of homogeneous catalytic hydrogenation using anion-promoted metal clusters. *J. Am. Chem. Soc.* **1986**, *108*, 4669–4671.

8. Adams, R.D.; Babin, J.E.; Tasi, M.; Wang, J.G. Catalyst design. The activation of a trinuclear metal cluster complex by metal atom substitution. *Organometallics* **1988**, *7*, 755–764.

9. Blomstrand, W. Ueber unorganische Haloidverbindungen, die sich wie Radicale verhalten. *J. Prakt. Chem.* **1859**, *77*, 88–119.

10. Schafer, H.; Schnering, H.G.; Tillack, J.; Kuhnen, F.; Wohrle, H.; Baumann, H. Neue Untersuchungen über die Chloride des Molybdäns. *Z. Anorg. Allg. Chem.* **1967**, *353*, 281–310.

11. Lee, S.C.; Holm, R.H. Nonmolecular metal chalcogenide/halide solids and their molecular cluster analogues. *Angew. Chem. Int. Ed. Engl.* **1990**, *29*, 840–856.

12. Cotton, F.A.; Hughbanks, T.; Runyan, C.E., Jr., Wojtczak, W.A. Halide-suppored octahedral clusters of zirconium: Structural and bonding questions. In *Early Transition Metal Clusters with π-Donor Ligands*; Chisholm, M.H., Ed.; VCH Publishers: New York, NY, USA, 1995; Chapter 1, p. 1.

13. Saito, T. Chalcogenide cluster complexes of the early transition metals. In *Early Transition Metal Clusters with π-Donor Ligands*; Chisholm, M.H., Ed.; VCH Publishers: New York, NY, USA, 1995; Chapter 3, p. 63.

14. Muetterties, E.L. Metal clusters in catalysis VIII. Reduction of triple bonds. *Bull. Soc. Chim. Belg.* **1976**, *85*, 451–470.

15. Struss, A.W.; Corbett, J.D. Reaction of hydrogen with metallic and reduced halides. The requirement of delocalized electrons for reaction. *Inorg. Chem.* **1978**, *17*, 965–969.

16. Imoto, H.; Corbett, J.D.; Cisar, A. Synthesis by hydrogen-driven disproportionation reactions. Synthesis and structure of the hexazirconium dodecahalide clusters Zr_6Cl_{12} and Zr_6Br_{12} and the double salt $Zr_6Cl_{12}.M_2ZrCl_6$ (M = sodium, potassium, cesium). *Inorg. Chem.* **1981**, *20*, 145–151.

17. Miller, G.J. Chemistry and properties of novel niobium cluster compounds. *J. Alloys Compd.* **1995**, *229*, 93–106.

18. Boorman, P.M.; Chong, K.; Jasim, K.S.; Kydd, R.A.; Lewis, J.M. A study of supported molybdenum cluster complexes as catalyst precursors: Part II. Evaluation of the catalytic activity of clusters supported on γ-alumina and fluorided γ-alumina. *J. Mol. Catal.* **1989**, *53*, 371–380.

19. Prokopuk, N.; Shriver, D.F. The octahedral M_6Y_8 and M_6Y_{12} clusters of group 4 and 5 transition metals. *Adv. Inorg. Chem.* **1999**, *46*, 1–49.

20. Kamiguchi, S.; Mori, T.; Watanabe, M.; Suzuki, A.; Kodomari, M.; Nomura, M.; Iwasawa, Y.; Chihara, T. Retention of the octahedral metal framework of Nb and Mo halide clusters in catalytic decomposition of phenyl acetate to phenol and ketene. *J. Mol. Catal. A* **2006**, *253*, 176–186.

21. Guggenberger, L.J.; Sleight, A.W. Structural and bonding characterizations of molybdenum dibromide, $Mo_6Br_{12}\cdot2H_2O$. *Inorg. Chem.* **1969**, *8*, 2041–2049.

22. Nannelli, P.; Block, B.P. Molybdenum(II) halides. *Inorg. Synth.* **1970**, *12*, 170.

23. Kamiguchi, S.; Kondo, K.; Kodomari, M.; Chihara, T. Catalytic ring-attachment isomerization and dealkylation of diethylbenzenes over halide clusters of group 5 and group 6 transition metals. *J. Catal.* **2004**, *223*, 54–63.

24. Nagashima, S.; Kamiguchi, S.; Ohguchi, S.; Chihara, T. Gas-phase alkylation of pyridine and phenol with alcohols over halide clusters of group 5–7 transition metals as solid acid catalysts. *J. Clust. Sci.* **2011**, *22*, 647–660.

25. Brosset, C. The structure of complex compounds of bivalent molybdenum. III. X-ray analysis of the structure of the chloro acid in alcohol solution. *Arkiv. Kemi.* **1949**, *1*, 353.

26. Johnson, O. Acidity and polymerization activity of solid acid catalysts. *J. Phys. Chem.* **1955**, *59*, 827–831.

27. Benesi, H.A. Acidity of catalyst surfaces. I. Acid strength from colors of asdorbed indicatios. *J. Am. Chem. Soc.* **1956**, *78*, 5490–5494.

28. Greenop, M.W.; Thomas, C.B. Nitration of alkylbenzenes catalyzed by mercury(II), thallium(III) and lead(IV). *J. Chem. Soc. Perkin Trans.* **1995**, *2*, 1595–1599.

29. Mashima, K. Catalytic diversity of diene complexes of niobium and tantalum on polymerizations of ethylene, norbornene, and methyl methacrylate. *Macromol. Symp.* **2000**, *159*, 69–76.

30. Bennett, M.A.; Matheson, T.W. Catalysis by ruthenium compounds. In *Comprehensive Organometallic Chemistry*; Wilkinson, G., Stone, F.G.A., Abel, E.W., Eds.; Plenum Press: Oxford, UK, 1982; Volume 4, p. 931.

31. Chen, X.; Zhang, T.; Zheng, M.; Wu, Z.; Wu, W.; Li, C. The reaction route and active site of catalytic decomposition of hydrazine over molybdenum nitride catalyst. *J. Catal.* **2004**, *224*, 473–478.

32. Kamiguchi, S.; Noda, M.; Miyagishi, Y.; Nishida, S.; Kodomari, M.; Chihara, T. Catalytic isomerization of 1-hexene to 2-hexene by halide clusters of Nb, Mo, Ta and W possessing an octahedral metal core. *J. Mol. Catal. A* **2003**, *195*, 159–171.

33. Kamiguchi, S.; Nagashima, S.; Komori, K.; Kodomari, M.; Chihara, T. Thermal activation of molecular tungsten halide clusters with the retention of an octahedral metal framework and the catalytic dehydration of alcohols to olefins as a solid acid catalyst. *J. Clust. Sci.* **2007**, *18*, 414–430.

34. Kamiguchi, S.; Nishida, S.; Kurokawa, H.; Miura, H.; Chihara, T. T. Formation of Brønsted acid site on halide clusters of group 5 and 6 transition metals. Catalytic methylation and demethylation of methylbenzenes with methanol. *J. Mol. Catal. A* **2005**, *226*, 1–9.

35. Simon, A.; Schnering, H.G.; Wöhrle, H.; Schäfer, H. Nb₆Cl₁₄–Synthese, Eigenschaften, Struktur. *Z. Anorg. Allg. Chem.* **1965**, *339*, 155.

36. Harder, K.; Preetz, W. Schwingungsspektren der Clusterverbindungen $(M_6X^i_{12})X^a_2 \cdot 8H_2O$, M = Nb, Ta; X^i = Cl, Br; X^a = Cl, Br, I. *Z. Anorg. Allg. Chem.* **1990**, *591*, 32–40.

37. Schoonover, J.R.; Zietlow, T.C.; Clark, D.L.; Heppert, J.A.; Chisholm, M.H.; Gray, H.B.; Sattelberger, A.P.; Woodruff, W.H. Resonance Raman spectra of $[M_6X_8Y_6]^{2-}$ cluster complexes (M = Mo, W; X, Y = Cl, Br, I). *Inorg. Chem.* **1996**, *35*, 6606–6613.

38. Kamiguchi, S.; Takahashi, I.; Kurokawa, H.; Miura, H.; Chihara, T. Vapor-phase synthesis of 1,2-dihydro-2,2,4-trimethylquinolines from anilines and acetone over group 5–7 metal halide clusters as catalysts. *Appl. Catal. A* **2006**, *309*, 70–75.

39. Kamiguchi, S.; Takaku, S.; Kodomari, M.; Chihara, T. Variable catalytic behavior of Nb, Mo, Ta, W, and Re halide clusters. Isomerization of alkynes to conjugated dienes under nitrogen and hydrogenation to alkenes under hydrogen. *J. Mol. Catal. A* **2006**, *260*, 43–48.

40. Kamiguchi, S.; Watanabe, M.; Kondo, K.; Kodomari, M.; Chihara, T. Catalytic dehydrohalogenation of alkyl halides by Nb, Mo, Ta, and W halide clusters with an octahedral metal framework and by a Re chloride cluster with a triangular metal framework. *J. Mol. Catal. A* **2003**, *203*, 153–163.

41. Cotton, F.A.; Wilkinson, G.; Murillo, C.A.; Bochemann, M. *Advanced Inorganic Chemistry*, 6th ed., Wiley: New York, NY, USA, 1999; p. 981.

42. Cotton, F.A.; Lippard, S.J.; Mague, J.T. Preparation and spectra of some adducts of the nonachlorotrirhenium and nonabromotrirhenium groups; evidence for the Re₃Br₉ group. *Inorg. Chem.* **1965**, *4*, 508–514.

43. Nagashima, S.; Kamiguchi, S.; Chihara, T. Halide cluster catalysis. Catalytic reactions. *Metals*, submitted for publication, 2014.